

Moisture plumes above thunderstorm anvils and their contributions to cross-tropopause transport of water vapor in midlatitudes

Pao K. Wang

Department of Atmospheric and Oceanic Sciences, University of Wisconsin-Madison, Madison, Wisconsin, USA

Received 28 May 2002; revised 1 December 2002; accepted 15 January 2003; published 28 March 2003.

[1] Water vapor in the lower stratosphere may play significant roles in the atmospheric radiative budget and atmospheric chemistry; hence it is important to understand its transport process. The possibility of water vapor transport from the troposphere to the stratosphere by deep convection is investigated using three-dimensional, nonhydrostatic, quasi-compressible simulations of a Midwest severe thunderstorm. The results show that the breaking of gravity waves at the cloud top can cause cloud water vapor to be injected into the stratosphere in the form of plumes above a thunderstorm anvil. Meteorological satellites and aircrafts have observed such plumes previously, but the source of water vapor and the injection mechanism were not identified. The present results reveal that there are two types of plumes, anvil sheet plumes and overshooting plumes, in this injection process and that the process is diabatic. A first-order estimate of this plume transport of water vapor per day from the upper troposphere to the lower stratosphere was made assuming that all thunderstorms behave the same as the one simulated. Other trace chemicals may also be similarly transported by the same mechanism. *INDEX TERMS*: 0341 Atmospheric Composition and Structure: Middle atmosphere—constituent transport and chemistry (3334); 3314 Meteorology and Atmospheric Dynamics: Convective processes; 3362 Meteorology and Atmospheric Dynamics: Stratosphere/troposphere interactions; *KEYWORDS*: cross-tropopause exchange, anvil top plumes, stratosphere-troposphere exchange of water vapor, moisture in the stratosphere, gravity wave breaking, cloud top gravity waves

Citation: Wang, P. K., Moisture plumes above thunderstorm anvils and their contributions to cross-tropopause transport of water vapor in midlatitudes, *J. Geophys. Res.*, 108(D6), 4194, doi:10.1029/2002JD002581, 2003.

1. Introduction

[2] Water vapor is important to the radiative budget of the atmosphere, and hence to climate studies, because of its strong absorption of infrared (IR) radiation [e.g., *Liou*, 1992; *Goody and Yung*, 1989]. It is also the main source of ozone-destroying HO_x radicals in the lower stratosphere. In the condensed phase, as exemplified by the recently observed anvil-top plumes [*Setvak and Doswell*, 1991; *Levizzani and Setvak*, 1996] to be discussed in detail later, it serves as a catalytic surface for heterogeneous reactions involving NO_x and halogen species [e.g., *Solomon*, 1999]. It is clear that the distribution of water substance in the upper troposphere/lower stratosphere (UT/LS) region has significant impacts on the global climate process.

[3] If the stratospheric water vapor concentration is not steady state, then its implications for climatic change must be carefully considered. A recent finding by *Oltmans et al.* [2000], using balloon-borne frostpoint hygrometers, shows that the stratospheric water vapor concentrations measured at two midlatitude locations (Washington, DC and Boulder, Colorado) have increased by 1–1.5% yr⁻¹ for the past 35 years, making the climatic impact of stratospheric water

vapor even more likely. The distribution of water vapor in the UT/LS is of special interest because this region is strongly influenced by the dynamics of stratospheric-tropospheric exchange, both diabatically and adiabatically, and may be chemically perturbed by subsonic aircraft emissions [*Pan et al.*, 1997].

[4] In order to assess the impact of water vapor, we need to understand how it is transported in the stratosphere. *Holton et al.* [1995] proposed that the global scale transport of water vapor in the lower stratosphere is due to the extratropical pumping mechanism generated by breaking Rossby waves and related potential-vorticity-transporting motions in the midlatitude atmosphere. In this scenario, the main source of lower stratospheric water vapor is the deep tropical convective clouds that pump water vapor from the troposphere to the stratosphere. In situ observations of convective storms and tropical cyclones confirmed the transport of lower tropospheric air into the lower tropical stratosphere [e.g., *Danielsen*, 1993]. Oxidation of methane may represent a minor water vapor source in the lower stratosphere. The tropical stratospheric water vapor is then transported poleward by the midlatitude “pumps” so that the middle and higher latitudes are basically a water vapor sink. *Plumb and Eluszkiewicz* [1999] proposed some modifications of the extratropical pumping mechanism but the main water vapor transport scheme remains the same.

[5] However, there are also seasonal and hemispheric variations of lower-stratospheric water vapor that cannot be explained by the mean circulation scenario alone. For example, aircraft measurements done by *Foot* [1984] over 45–65°N indicated that the midlatitude lower-stratospheric water vapor concentration is much higher than can be explained solely by tropical entry of air. Also, results of ER-2 research aircraft measurements during the Airborne Antarctic Ozone Experiment (AAOE) and the Airborne Arctic Stratospheric Expedition (AASE) showed that the wintertime water vapor fields in the lower stratosphere display a hemispheric asymmetry, with much lower early spring values in the Southern Hemisphere (SH) than the Northern Hemisphere (NH) [*Kelly et al.*, 1990]. Export of dehydrated air from the polar vortex was investigated as the possible mechanism for the asymmetry.

[6] Using water vapor data from the Stratospheric Photochemistry, Aerosols and Dynamics Expedition (SPADE), *Hintsas et al.* [1994] found higher water vapor concentration in the NH in fall than in spring. *Pan et al.* [1997], using Stratospheric Aerosol and Gas Experiment II (SAGE II) data, found a strong seasonal cycle of the water vapor mixing ratio on the 320K isentropic surfaces for both hemispheres, with maximum values in summer and minimum values in early spring. By also analyzing SAGE II ozone data, they inferred from both water vapor and ozone data that extratropical UT/LS exchange has a significant influence on the lowermost stratosphere, especially in the NH summer season.

[7] *Rosenlof et al.* [1997] analyzed both the Halogen Occultation Experiment (HALOE) satellite water vapor measurements and in situ aircraft measurements, and explained the above-mentioned NH-SH asymmetry and seasonal variations by the nature of global circulations in NH and SH. For example, during the tropical dry period (December, January, and February), dry air initially spread to both hemispheres. However, the stronger NH wintertime descent that exists relative to that of SH summer transport the dry air out of NH lower stratosphere more quickly than in the south. This same hemispheric asymmetry in winter descent brings down a greater quantity of “older” higher water vapor content air in the north, which also acts to moisten the NH lower stratosphere relative to the SH.

[8] *Dunkerton* [1995] used 21 years (1973–1993) of rawinsonde data together with 8 years (1985–1992) of uninitialized European Center for Medium-Range Weather Forecast (ECMWF) analyses to study the climatological structure of large scale circulations adjacent to monsoon regions in NH and SH summers. He concluded that there are significant meridional velocities ($>1 \text{ m s}^{-1}$) in the UT/LS that can transport constituents horizontally from the troposphere into the lower stratosphere in the Asian and Mexican monsoon regions. These NH monsoon regions are further displaced from the equator than the SH monsoons, and hence provide a possible explanation for the aforementioned seasonal cycle and NH-SH asymmetry of the lower stratospheric water vapor. *Chen* [1995] used 9 years (1985–1993) of ECMWF global analysis data and a two-dimensional semi-Lagrangian transport model to investigate the transport of tracers along the isentropic surfaces that intersect the tropopause. His results provided further evidence of the

transport of tropospheric air (and presumably with a certain amount of water vapor) to the lower stratosphere.

[9] The transport mechanisms discussed in the above paragraphs are all large-scale in nature. It is desirable to understand these transport mechanisms in smaller scale so that finer physical processes involved can be identified. Understanding these processes in smaller scale not only helps to clarify the transport mechanisms, but also provides conceptual basis for in situ aircraft measurements. Furthermore, such knowledge will afford modelers to perform quantitative computations so as to obtain more accurate estimates and better transport parameterizations for global models.

[10] The paper proposes a cloud-scale mechanism that can transport atmospheric constituents (including water vapor) from the troposphere to the stratosphere. Unlike the studies of *Dunkerton* [1995] and *Chen* [1995], both of which concern adiabatic (isentropic) transport, this is a diabatic mechanism that is associated with the breaking of gravity waves at the tops of deep convective storms in the middle latitudes. To illustrate this mechanism, a three-dimensional cloud dynamical model with detailed cloud microphysics package was utilized to perform a simulation study of a typical High Plains supercell storm. The model results are used to demonstrate this transport process.

[11] In the following sections, I will first describe briefly the cloud model used for this study. Next, I will discuss the general conditions and relevant observational facts about the supercell storm selected for this study, followed by a discussion on the comparison between model results and observation so as to validate the simulation results. Then I will provide a detailed discussion on the proposed mechanism as shown by the simulation results, along with some supporting evidence for this theory from satellite observations. The implications of this transport mechanism on the UT/LS water vapor and other constituents will then be discussed. A conclusion section will be given at the end.

2. Description of the Cloud Model WISCDYMM

[12] The tool utilized for the present study is the Wisconsin Dynamical/Microphysical Model (WISCDYMM), which is a three-dimensional, quasi-compressible, time-dependent, non-hydrostatic primitive-equation cloud model developed at the University of Wisconsin-Madison by the author’s research group. The following subsections provide a brief description of the model.

2.1. Model Numerics

[13] WISCDYMM incorporates time-dependent, non-hydrostatic primitive equations cast in quasi-compressible form adopted from *Anderson et al.* [1985]. Twelve dependent variables are predicted including the velocity components in the x-, y-, and z-directions (u , v , w), pressure (p), potential temperature (θ), turbulent kinetic energy per unit mass (E), water vapor (q_v), cloud water (q_c), cloud ice (q_i), rain water (q_r), snow aggregates (q_s), and graupel/hail (q_h) as given by *Straka* [1989].

[14] In this study, the model uses an Arakawa-C staggered grid [*Arakawa and Lamb*, 1981]. The horizontal domain is $55 \times 55 \text{ km}^2$ with 1-km grid resolution. There are 40 grid cells in the vertical domain with a spacing of 200

m from surface (250 m) up to 20 km. A sensitivity run in which the top boundary was set a 30 km produced very similar results. The following analysis is based on the 20 km top surface results. The forward-in-time upstream sixth-order Crowley scheme, as recommended by *Tremback et al.* [1987], is used for advection terms. The prognostic model variables are filtered every model time step with a fourth-order spatial smoother similar to that used by *Klemp and Wilhelmson* [1978a]. A time filter of *Asselin* [1972] is applied lightly, with a coefficient of 0.125, to all prognostic variables to couple the leapfrog solutions from odd and even time steps. The lateral boundaries incorporate “radiative” open boundary conditions that allow disturbances to pass smoothly out of the domain [*Klemp and Wilhelmson*, 1978a]. At the top boundary, all variables are held at their base-state values. A Rayleigh sponge layer is installed from 17 to 20 km in order to absorb the energy of upward-propagating gravity waves generated by the convection. The intrinsic gravity wave speed used in the radiative lateral boundary condition is 40 m s^{-1} .

2.2. Model Microphysics

[15] The microphysical processes are parameterized by the bulk method with water substance categorized into six types: water vapor, cloud water, cloud ice, rain, snow, and graupel/hail. The model incorporates 38 microphysical processes including nucleation, condensation, evaporation, freezing, melting, sublimation, deposition, autoconversion and accretion. The governing equations and parameterization expressions are given in *Straka* [1989]. The Hail Parameterization Model (HPM) version of WISCDYMM, which is the one used for this study, assumes inverse exponential size distributions for rain [*Marshall and Palmer*, 1948], snow [*Gunn and Marshall*, 1958], and graupel/hail [*Federer and Waldvogel*, 1975]. The cloud water is assumed to be monodispersed with a number concentration as a function of location, while cloud ice is assumed to be monodispersed as a function of temperature. Each class of precipitation is assumed to fall with its mass-weighted mean terminal fall speed relative to the air. A complete description is given by *Straka* [1989].

[16] The equations for the model microphysics are primarily based on those of *Lin et al.* [1983] and *Cotton et al.* [1982, 1986] and are given by *Straka* [1989]. Mixing ratios are used to represent all hydrometeors, with base-state values of zero. Negative moisture values are allowed but are not used in the microphysical calculations. This procedure is used to help prevent spurious increases in total moisture, which occur when negative values of the mixing ratios are reset to zero. In the present study, negative moisture values are rare and their magnitudes are insignificant. All hydrometeors in the model are assumed to be spherical, except that cloud ice crystals are assumed to be hexagonal plates.

2.3. Model Initiation and Reference Frame

[17] Convection in the model is initiated by a technique similar to that used by *Klemp and Wilhelmson* [1978a] and *Straka* [1989]. A warm thermal bubble 20 km wide and 4 km deep is centered 2 km above ground level (AGL) in a horizontally homogeneous environment. The maximum thermal perturbation is 3.5 K in the center of the bubble,

and the mixing ratio is adjusted to keep the relative humidity (RH) the same as that in the undisturbed sounding. In order to keep the active convection within the $55 \times 55 \times 20 \text{ km}^3$ domain during the simulation, a mean horizontal wind is removed from the earth-relative base-state wind profile and is adjusted every 30 min, depending on the storm movement, to accommodate changes as the convective system propagates. The removed mean horizontal wind can be decided from the location of the maximum updraft in the second part of model statistics output file. A 3-s time step was used in the model simulations and the output was analyzed every two minutes.

3. The 2 August 1981 CCOPE Supercell

[18] The storm chosen for the simulation for illustrating the plume-formation mechanism is a supercell that passed through the center of the Cooperative Convective Precipitation Experiment (CCOPE) [*Knight*, 1982] observational network in southeastern Montana on 2 August 1981. The storm and its environment were intensively observed for more than 5 h by a combination of seven Doppler radars, seven research aircraft, six rawinsonde stations and 123 surface recording stations as it moved east-southeastward across the CCOPE network. *Miller et al.* [1988] and *Wade* [1982] provided many of the observations in this section, especially those on the history of the storm. This case was chosen because it is a typical deep convective storm in the US High Plains and it provides much detailed observational data for comparison with model results with regard to dynamics and cloud physics, and the author’s group has obtained successful simulations of it previously [*Johnson et al.*, 1993, 1994].

3.1. Environmental Conditions

[19] The initial conditions for the simulation are based on a 1746 MDT (Mountain Daylight Time) sounding (Figure 1) taken at Knowlton, Montana, approximately 90 km ahead of the storm. This sounding provided the most representative temperature and moisture profile available, with a massive convective available potential energy (CAPE) 3312 J kg^{-1} distributed over a comparatively shallow layer from the level of free convection LFC = 685 mb to the equilibrium level EL = 195 mb. The subcloud layer (below 730 mb) was nearly dry-adiabatic and well mixed, with a potential temperature close to 311.5 K, and also relatively moist because a surface low in north central Wyoming advected water vapor mixing ratios of 12–13 g kg^{-1} into the region on easterly winds. Above the subcloud region, a strong capping dry layer existed at approximately 710 mb, caused by warmer and drier air that had unexpectedly moved into the region after 1300 MDT. *Wade* [1982] gives some possible causes of this warming. The dry layer was significant in that it allowed the low-level air mass to continue warming for the remainder of the afternoon and become even more potentially unstable. From the dry layer to 450 mb, the environmental lapse rate was nearly dry adiabatic. The calculated indices from the Knowlton sounding (Total Totals index = 60, Lifted index = -9.4, and a K index = 38) indicated that the air mass over

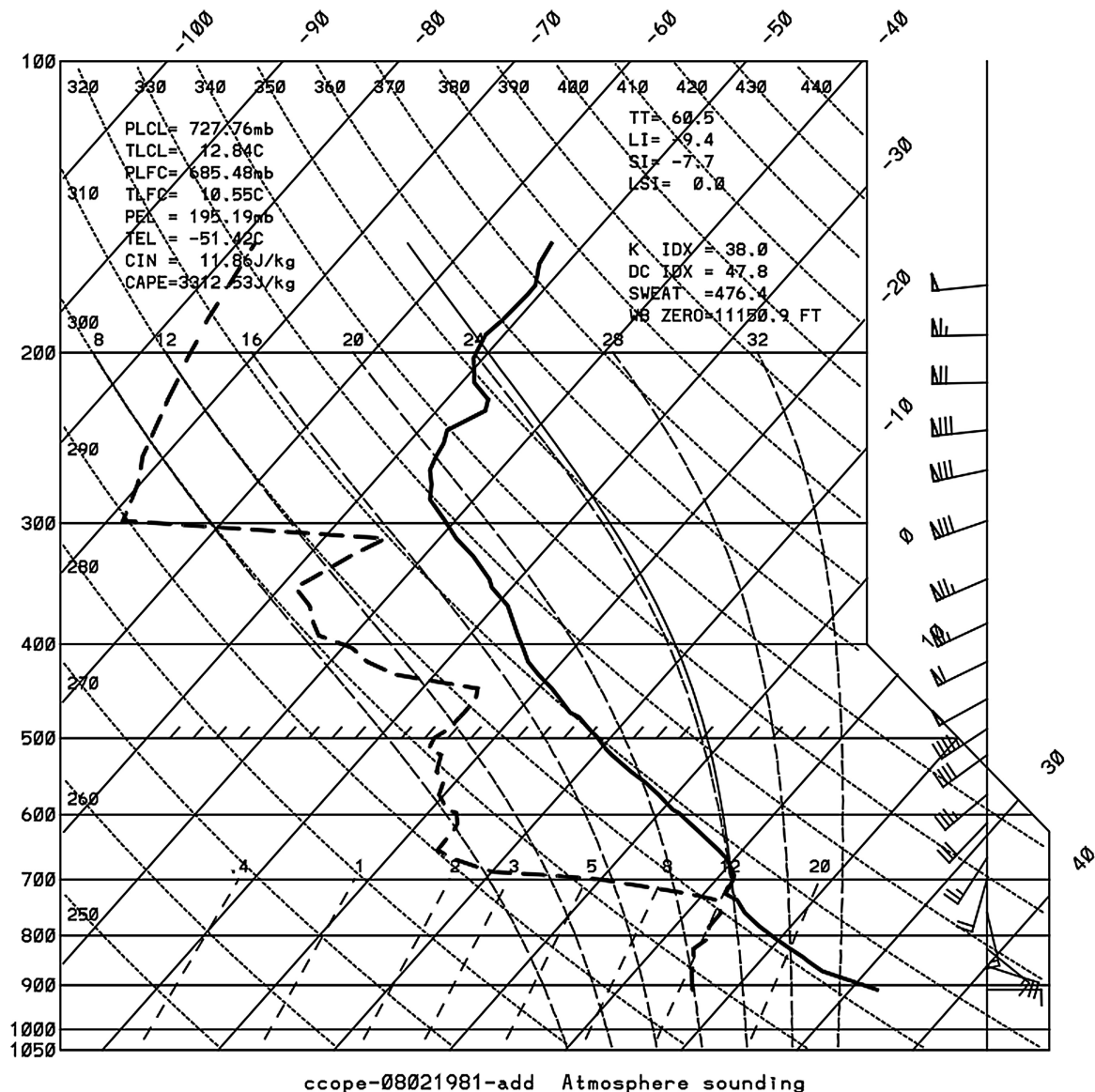


Figure 1. The 1746 MDT Knowlton, Montana sounding on 2 August 1981. The solid curve is for temperature and dashed curve for dew point. The portion of dew point curve above 300 hPa, which was missing in the original sounding, is constructed using an average August 1999 HALOE water vapor profile over 40–60N.

eastern Montana on 2 August was very unstable, and hence very favorable for the development of deep convection.

[20] Large vertical wind shear between lower and mid-levels was also conducive to severe weather development. The 1746 MDT Knowlton hodograph (not shown) indicated strong subcloud flow, veering nearly 70° from the surface layer to cloud base at 1.6 km AGL. The magnitude of the mean shear over the lowest 6 km was 0.008 s^{-1} [Weisman *et al.*, 1983]. There was little directional shear above the cloud base, but vertical speed shears between the cloud base and 9 km were 0.006 s^{-1} [Miller *et al.*, 1988]. Taking into account the vertical wind shear and buoyancy effects, the Bulk Richardson Number for the pre-storm environment was 25, in the expected range for supercell storms [Weisman and Klemp, 1982]. As explained by Klemp and Wilhelmson [1978b], clockwise curvature of the wind shear vector over

the lowest 2 km of the hodograph also favored development of the right-moving supercell.

3.2. Grid Resolution and Treatment of Model Initialization

[21] Johnson *et al.* [1994] simulated this supercell using a grid cell size of $1 \times 1 \times 0.5 \text{ km}^3$ in order to understand its bulk dynamics and physics. The results of this simulation indicated that the overall dynamics and microphysics were simulated well at this resolution. However, since the main concern in the present study is the transport of water vapor, it is meaningful to test the model sensitivity to grid resolution. For this purpose, three different resolutions were tested: $1 \times 1 \times 0.5 \text{ km}^3$, $1 \times 1 \times 0.2 \text{ km}^3$, and $0.5 \times 0.5 \times 0.2 \text{ km}^3$. All three sets of results show the plume phenomenon clearly, and plume characteristics are similar from run

Table 1. Comparison of Various Dynamical and Microphysical Quantities Between the Observed CCOPE Supercell and the Simulated Storm

Feature	Observation	Simulation
Anvil extent downstream from updraft	>200 km	>150 km (estimate)
Anvil extent upstream from updraft	>20 km	>20 km
BWER diameter	7 km	6–7 km
BWER vertical extent	7.5 km	7.0 km
Cloud base height	1.5 km	1.6 km
Cloud ice mixing ratio (mid-levels)	2 g kg ⁻¹	2 g kg ⁻¹
Cloud top height	14–15 km	14–15 km
Cloud water body diameter	8 km	8–9 km
Cloud water drop size in BWER	6 μm	4–5 μm
Cloud water mixing ratio (mid-levels)	3–4 g kg ⁻¹	3–4 g kg ⁻¹
Downdraft velocity (mid-levels)	12 m s ⁻¹	8 m s ⁻¹
Gust front location from updraft	S and E	S and E
Gust front wind velocity	>20 m s ⁻¹	>20 m s ⁻¹
Typical hail diameters at surface	10–30 mm	5–20 mm
Max. hail diameter at surface	8.8 cm	7.3 cm
Hail shaft location from BWER	3–4 km W	3–4 km NW
Lifetime of supercell features	> 2 hr	> 2hr
Low-level hook echo position	SE flank	SE flank
Low-level vorticity initiation	After 1700 MDT	After 60 min
Rainfall totals (maximum)	30–35 mm	28–36 mm
Reflectivities (maximum)	62–72 dBZ	62–65 dBZ
Reflectivities at surface	55–65 dBZ	55–65 dBZ
Reflectivities in BWER	<35 dBZ	<45 dBZ
Storm movement (development stage)	260 at 10 m s ⁻¹	247 at 11 m s ⁻¹
Storm movement (supercell stage)	282 at 18 m s ⁻¹	265 at 14 m s ⁻¹
Storm top overshoot above tropopause	2–3 km	2–3 km
θ _c in low-level cold pool	320–325 K	320–325 K
θ _c in updraft core	348–350K	345–350K
Updraft diameter	14–17 km	14–16 km
Updraft velocities (maximum)	50–55 m s ⁻¹	60 m s ⁻¹
Vertical vorticity in mid-levels	0.01 s ⁻¹	0.015 s ⁻¹
Peak vertical vorticity from peak updraft	5 km S	3.5 km SE

to run The refined vertical resolution results reveal more detailed plume structure, but even the lowest resolution case simulated the plume formation well. The only notable difference between the latter two cases is that the one with refined horizontal resolution shows more detailed midlevel horizontal structure. Since the utmost concern of this study is the vertical transport, it was decided to choose the simulation results with the refined vertical but lower horizontal resolution (1 × 1 × 0.2 km) for analysis here. The smaller data set of this run can be analyzed more efficiently while preserving the accuracy of the results. Table 1 shows the comparison between the dynamical and microphysical characteristics of the observed and simulated storms using this grid resolution. It is seen that they agree reasonably well with each other, and better than that reported by *Johnson et al.* [1994].

[22] It is worthwhile to note that the original 1746 MDT Knowlton, Montana sounding did not contain moisture information above 300 mb. The simulation of *Johnson et al.* [1994] was performed under the assumption of no water vapor above 300 mb initially. However, since the present study is concerned with water vapor transport, this assumption needs to be examined. To ensure that the upper-level (above 300 mb) moisture is properly represented, the average August 1999 Halogen Occultation Experiment (HALOE) water vapor profile over midlatitudes (40°–60°N) is added to represent the upper level humidity, as shown in Figure 1. It turned out that the results of the HALOE-modified case do not differ significantly from that

of *Johnson et al.* [1994]. The following discussions are based on the results of the HALOE-modified case.

4. Results and Discussions

[23] Although the present study is performed at higher grid resolution than that of *Johnson et al.* [1994], the overall bulk dynamical and microphysical behavior of the simulated storm are essentially the same as reported therein and hence will not be discussed here. Instead, we will focus on the cloud top features, especially the above-anvil plume phenomenon that is associated with the transport of water vapor from the troposphere to the stratosphere.

4.1. Central Cross-Section Features

[24] In the following discussions, the plume phenomenon in the simulated storm will be illustrated first using the fields of relative humidity with respect to ice saturation, RH_i, which is more relevant than the relative humidity with respect to liquid water, because ice is far more common at the cloud top temperatures. Since the relative humidity includes both the effects of vapor pressure and temperature, it approximates the appearance of the cloud better than the water vapor mixing ratio q_v , because a high RH means high probability of condensation. This is especially so when comparing with satellite images. However, the q_v profiles will be more appropriate for understanding the magnitude of water vapor transport in the UT/LS. Therefore, examples of q_v profiles will also be shown and discussed.

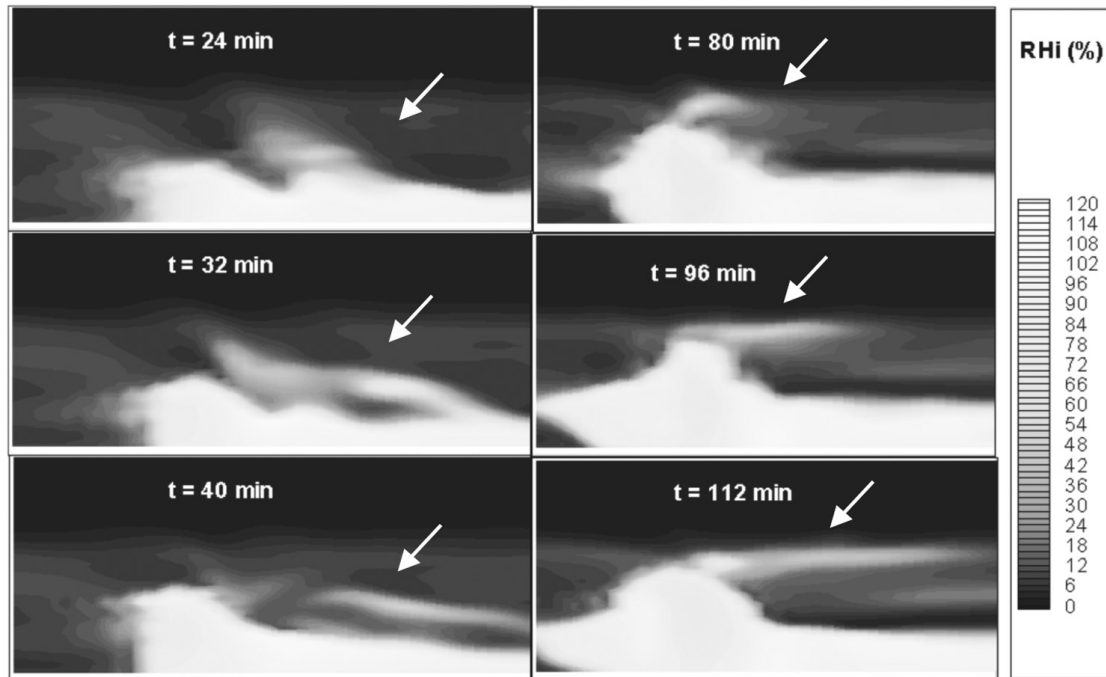


Figure 2. Snapshots of modeled RH_i (relative humidity with respect to ice) profiles at $t = 24, 32, 40, 80, 96$ and 112 min in the central east-west cross-section ($y = 27$ km), showing the plume feature above the anvil. Only the portion near the cloud top is shown. The vertical axis range is 10–20 km and horizontal axis range 20–55 km.

[25] The simulation results reveal that there are at least two different plume formation processes at the cloud top. The first, associated with the overshooting dome of the storm, will be called the “overshooting plume” for convenience. The second, associated with the breakaway of cloud top materials in the anvil sheet downstream from the updraft core, will be called the “anvil sheet plume” to distinguish it from the overshooting plume. In the present simulation the anvil sheet plume occurs earlier than the overshooting plume, but this order is not necessarily a rule, as it probably depends on the circumstances. As we will see later, both types of plumes are caused by the breaking of cloud top gravity waves.

[26] Figure 2 shows six panels of the RH_i profiles in the central east-west cross-section ($y = 27$ km) of the storm. This is where the storm development is normally (though not always) most vigorous. Since the cloud top region is the focus here, these snapshots are windowed to 10–20 km vertically and 20–55 km horizontally, with the vertical scale stretched in these views. Note also that all descriptions of distances and directions in the following discussions are storm-relative. During the computation, the simulated storm is moving east as did the actual CCOPE storm. In order to keep the storm in the computational domain, the mean storm motion has been subtracted from the wind field so that the simulated storm appears to be quasi-stationary in the resulting reference frame.

[27] No obvious plume structure is discernible before 24 min into the simulated storm activity. At 24 min, as shown in the first panel in Figure 2, strong gravity wave motions at the cloud top are visible. There is a large surge of comparatively high humidity (RH_i ~ 30 –50%) above the

second wave crest (to the east of the main updraft column) that seems to propagate upward and westward (i.e., upstream relative to the upper-level wind direction) into the stratosphere. At 32 min, this moist surge appears to be nearly detached from the anvil of the storm and form a separate moist layer in the stratosphere. The surge appears to consist of two parts, one to the west and one to the east. The one to the west (left) is less humid (RH_i ~ 40 %) and seems to merge with the overshooting dome later while the one to the east (right, RH_i ~ 50 –75%) becomes slightly elevated and develops into a separate plume above the storm anvil at 40 min. This plume, sloping slightly downward toward the downstream direction and almost parallel to the slope of the anvil, appears to gradually dissipate with time into a diffuse moist layer. Relative to the storm, the anvil sheet plume seems to propagate slightly upward and upstream, and may be responsible for the stratospheric cirrus observed by Fujita [1982, p. 362], who stated that “One of the most striking features seen repeatedly above the anvil top is the formation of cirrus cloud which jumps upward from behind the overshooting dome as it collapses violently into the anvil cloud.” The animation of plume formation at this stage matches this description very well.

[28] Note that the formation of the anvil sheet plume as described above could be a result of the model spin-up process in response to the original thermal perturbation used to initiate the convection. Hence, it may not necessarily have occurred in the actual CCOPE storm. However, this should not nullify the possibility of this process, as all it needs is vigorous gravity wave activity in the anvil sheet as can occur in any severe thunderstorm. Some thunderstorms may form anvil sheet plumes at later stages, as long as there

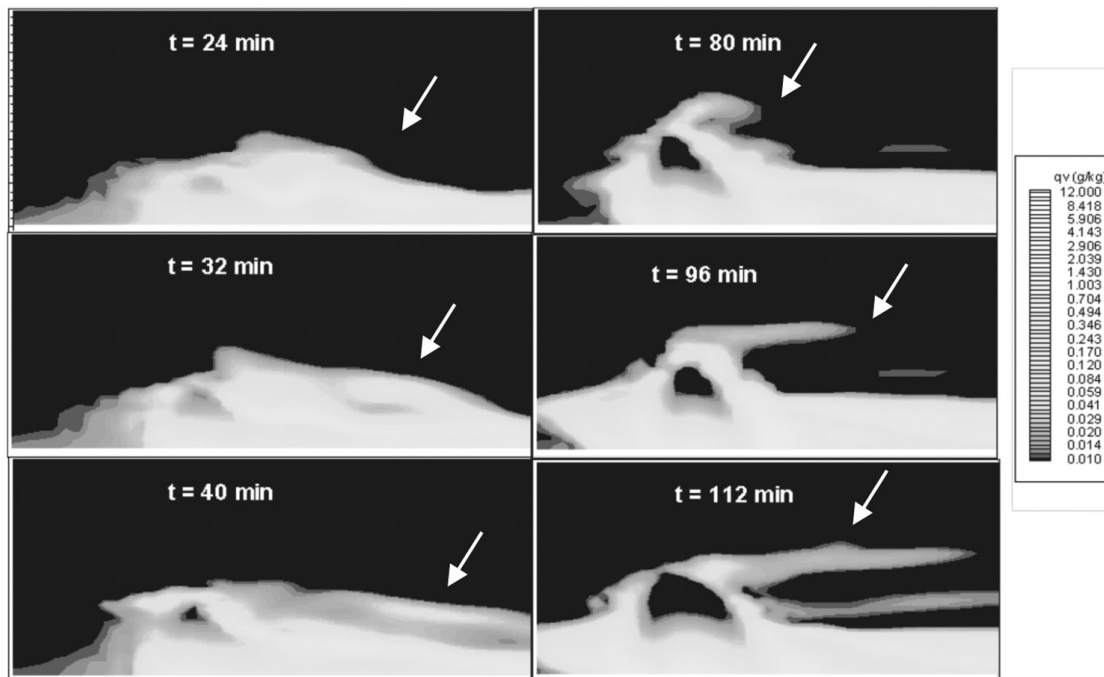


Figure 3. Same as Figure 2 except for modeled q_v profiles.

are strong instabilities in the cloud top region. The cloud top gravity wave phenomenon will be discussed in more detail later.

[29] Another stage of plume formation, the overshooting plume, starts at about 70 min into the simulation, as shown by the three snapshots on the right-hand-side in Figure 2. The RHi of the overshooting plume is generally much higher than that of the anvil sheet plume. At 80 min, a moist patch appears to emanate from the overshooting dome. Subsequently, it gradually takes on the shape of a chimney plume. The stretching of the plume downwind is apparently caused by the upper-level winds, which are predominantly westerlies. The maximum RHi in the core of the plume sometimes exceeds 100%. At 112 min, the plume has reached the east boundary of the computational domain and an altitude of 15–16 km. The altitude of the anvil sheet plume, in contrast, is 12–13 km. Thus there may be more than one layer of plumes at a given time. The precise thickness of plumes depends on the choice of RHi that defines their boundaries, but generally the thickness ranges from several hundred meters to about 1 km for $\text{RHi} \geq 10\%$. It is also seen from the figure that there is a shallow dry layer immediately above the anvil. This layer is about 1–1.5 km thick and apparently extends to the whole length of the anvil in the computational domain.

[30] Figure 3 shows snapshots of the q_v field for the same times and cross-sections as in Figure 2. The overall structure of the q_v field is similar to that of RHi even though the latter includes the effect of temperature. This indicates that the main mechanism for producing the features described in the preceding paragraph is due to the distribution of water vapor mixing ratio while temperature effect is secondary. However, the temperature effect becomes significant in the updraft core. The most notable difference between Figure 2 and Figure 3 is in the core area of the overshooting dome

where, unlike the more smoothly distributed RHi field, the values of q_v change rapidly, being very low in the core region and increasing rapidly outward. This water vapor structure can be explained as follows. The updraft brings the air from lower levels, relatively unaffected by the mixing with environmental air. Near the edges of the dome, on the other hand, the air is older as it has arrived at the cloud top sometimes earlier, it is descending (compare Figure 5), and it is already considerably mixed with the stratospheric air. Thus it is warmer (in potential temperature sense) and has higher q_v for the same RHi. Aside from the core region, the q_v field looks similar to the RHi field.

4.2. Three-Dimensional Cloud Top Features

[31] The discussions in the previous section are based on the plume features shown in the central vertical cross-sections of the storm. The single cross-sectional view obviously does not reveal the three-dimensional structure of the plume, which is shown in Figure 4. Here again, only the portion of the storm above 10 km is shown. Six snapshots of the cloud tops, represented here by the contour surface of $\text{RHi} = 30\%$, are shown as seen from above and northeast of the storm. The value 30% is chosen so that the physical characteristics of the plumes can be clearly examined. A choice of a higher RHi value results in somewhat smaller plumes whereas choosing a smaller RHi value results in somewhat larger plumes, but the main characteristics remain very much the same.

[32] As in Figure 2, the plume associated with the second wave crest becomes noticeable at $t = 24$ min. At $t = 32$ min, this plume becomes larger and moves both upward and upstream. It then recedes downstream afterward, as revealed by the image at $t = 40$ min, gradually dissipates, and becomes nearly invisible after 60 min. On the other hand, the plume associated with the overshooting top first become

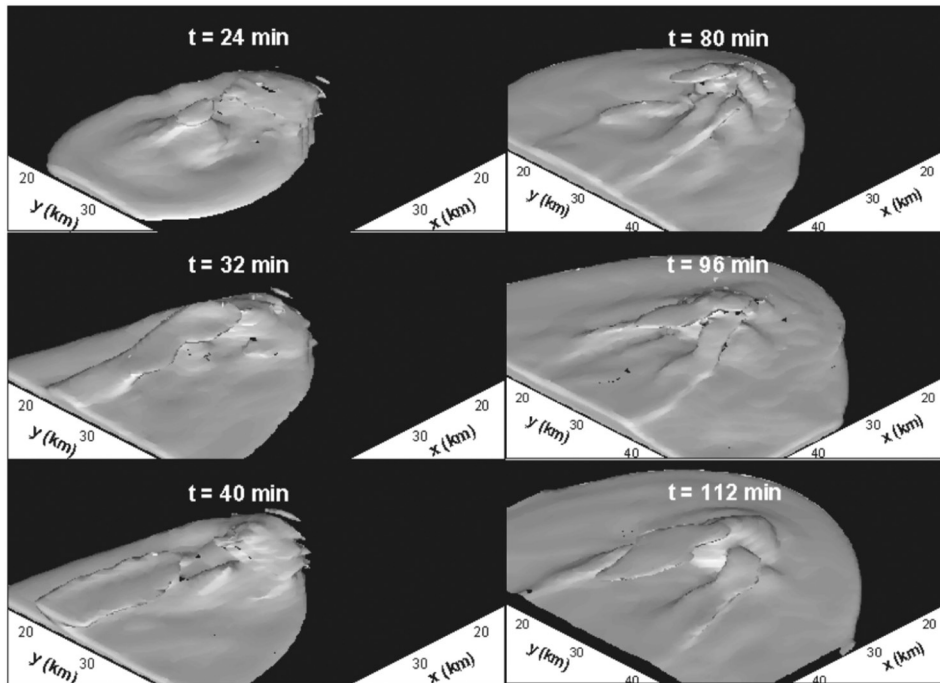


Figure 4. Snapshots of 3D renderings for the 30% RHi contour surface at $t = 24, 32, 40, 80, 96$ and 112 min, showing the plume features above the anvil. Data below 10 km are windowed out.

recognizable at 36 min at a level above the wave-crest plume. It fluctuates in size for a while, but becomes elongated into a chimney plume shape starting at ~ 80 min. The main orientation is along the upper-level wind, although there are slight meanders, probably due to the perturbation of the flow passing the overshooting dome.

[33] The snapshots at 80, 96, and 112 min also show that there is another plume-like structure at a lower level of the overshooting dome. It seems to emanate from a mid-level point and orient northeast in the beginning. This lower level plume is sometimes separated from the anvil below, although it eventually merges with the latter. Obviously, this side-protruding plume would not be revealed in the central cross-sectional view in Figures 2 and 3.

4.3. Mechanism of Plume Formation

[34] The snapshots of the RHi fields shown in Figures 2–4 suggest that the plumes form from the moisture ejected from the cloud below. Further, inspection of the morphology of cloud top structure and the analysis of the cloud top stability structure suggest that the moisture is detached from the cloud via the gravity wave breaking. This is explained below.

[35] The strong convection in a thunderstorm like this would set off vigorous gravity waves at the cloud top level. Several investigators have studied the dynamical behaviors of these convectively generated gravity waves. For example, *Clark et al.* [1986] performed two-dimensional numerical simulations to investigate the internal gravity waves excited by convection over an unstable boundary layer. They showed that even shallow convection could generate gravity waves that can propagate into the stratosphere. They argued that these gravity waves are excited by thermal forcing combined with the boundary layer eddies and cumulus clouds acting as obstacles to the flow in the

presence of mean environmental wind shear. If shallow convections can excite gravity waves, then deep convections should be able to excite even more vigorous gravity waves, as demonstrated by others. *Fovell et al.* [1992] studied the excitation and vertical propagation of gravity waves in a mesoscale convective storm using a two-dimensional model, and concluded that, in the absence of storm-relative mean winds, the mechanical forcing due to oscillatory updrafts is responsible for the excitation of the primary mode of these waves. *Alexander et al.* [1995] utilized a two-dimensional fully compressible nonlinear simulation of midlatitude squall line to study vertically propagating waves generated by deep convections. *Pandya and Alexander* [1999] compared the spectra of the gravity waves generated by a time-varying tropospheric thermal forcing representing organized convection to the spectra of stratospheric gravity waves reported by *Alexander et al.* [1995] and concluded that stratospheric gravity waves above convection can be understood primarily in terms of the linear response to a time- and space-dependent thermal forcing.

[36] There are obvious gravity waves excited in the present simulation. Figure 5 shows a snapshot of vertical velocity field in the storm central cross-section at $t = 40$ min. The pattern of vertical velocity field in the stratosphere clearly reveals the gravity wave activity. The strong gravity waves as well as the overshooting distort the initially horizontal tropopause. Figure 6 shows the central cross-section of the simulated storm at $t = 120$ min. Here the cloud top roughly coincides with the $\theta \sim 372\text{K}$ isosurface, which is severely distorted by the overshooting and the gravity waves. However, it is known that, if no wave breaking occurs, then there will be no net transport of material cross the isentropic surface however strong the

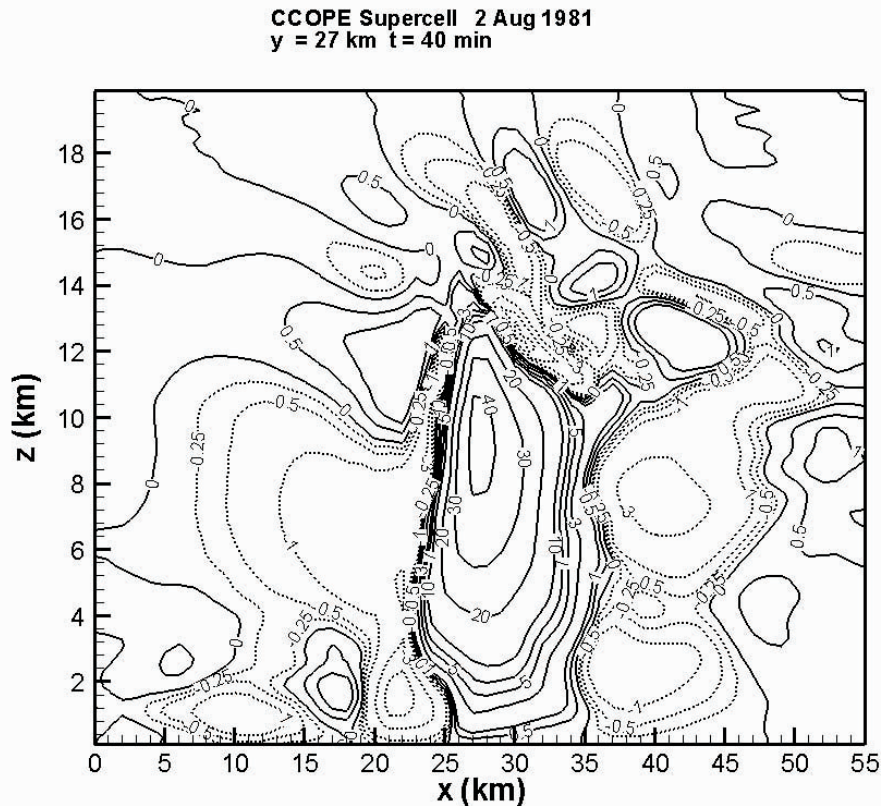


Figure 5. The vertical velocity (w) field in the central east-west cross-section of the simulated storm at $t = 40$ min. Solid (dotted) contours represent positive (negative) w (in m s^{-1}).

distortion may be [Holton *et al.*, 1995]. However, when the instability (and hence the turbulence level) at the cloud top becomes sufficiently high, wave breaking may occur.

[37] Figures 7 and 8 provide direct evidence of the wave breaking by the reversal of velocity vectors with height and the overturn of isentropes in the breaking areas. Figure 7 shows the occurrence of anvil sheet plumes at $t = 30$ min whereas Figure 8 shows the occurrence of overshooting plumes at $t = 73$ min 10 sec. The present model results also show that the ejection of moist parcels is non-adiabatic, as the motion evidently cuts through isentropic surfaces. It also cuts through the equivalent potential temperature surfaces (not shown) and hence is not moist-adiabatic either. However, once a parcel is detached from the main cloud body, it tends to follow the upper level winds and move along isentropic surfaces. Thus the non-adiabatic part of the process is in the detachment whereas the transport in the stratosphere is mainly adiabatic, especially when no phase change occurs.

4.4. Origin of the Plume Air

[38] Whereas the air in the overshooting plume appears to come from the overshooting dome, it cannot come from its core whose temperatures are generally very low. The cold temperature is mainly due to the expansion cooling of the rapidly ascending air in the dome, as the maximum updraft exceeds 60 m s^{-1} . As seen in Figures 4 and 5, at 32 min when the core starts to develop, the minimum temperature is about 205K and the corresponding q_v and RH_i are 0.012

g kg^{-1} and 91%, respectively. As time goes on, the core becomes drier and colder. At $t = 112$ min, the minimum temperature becomes 193K and the corresponding q_v and RH_i are 0.0024 g kg^{-1} and 79%, respectively.

[39] However, this cold dry core is enveloped by a relatively warm and moist shell whose temperature is about 15–25K warmer and with maximum q_v 10 to 30 times more than the core region. This shell is the source of water vapor for the plumes. The properties of the overshooting dome shell have been studied observationally by Roach [1967], who documented a photographic and radiometric study of the summit areas on several severe thunderstorms in Oklahoma as viewed from a U-2 aircraft at an altitude of 20 km. In an effort to reconcile the radiometer observations showing a cloud-top environment about $20 \sim 30^\circ\text{C}$ warmer than the core of the overshooting dome, he postulated the existence of a shell where mixing between the environment and the interior of the dome took place, with large gradients of temperature and hydrometeor concentrations, and therefore of opacity. Roach's scenario is confirmed by the present model results as illustrated in Figure 6. The downstream-going plume apparently originates from the overshooting dome shell and has a temperature of about 210K (-63°C). This is indeed about 20°C warmer than the dome core. It is seen that there is also a small protrusion of cold air of about 210K pointing to the upstream from the overshooting dome. It is possible that this protrusion could have become another plume that extends to the left in the case when the upper level winds are weak.

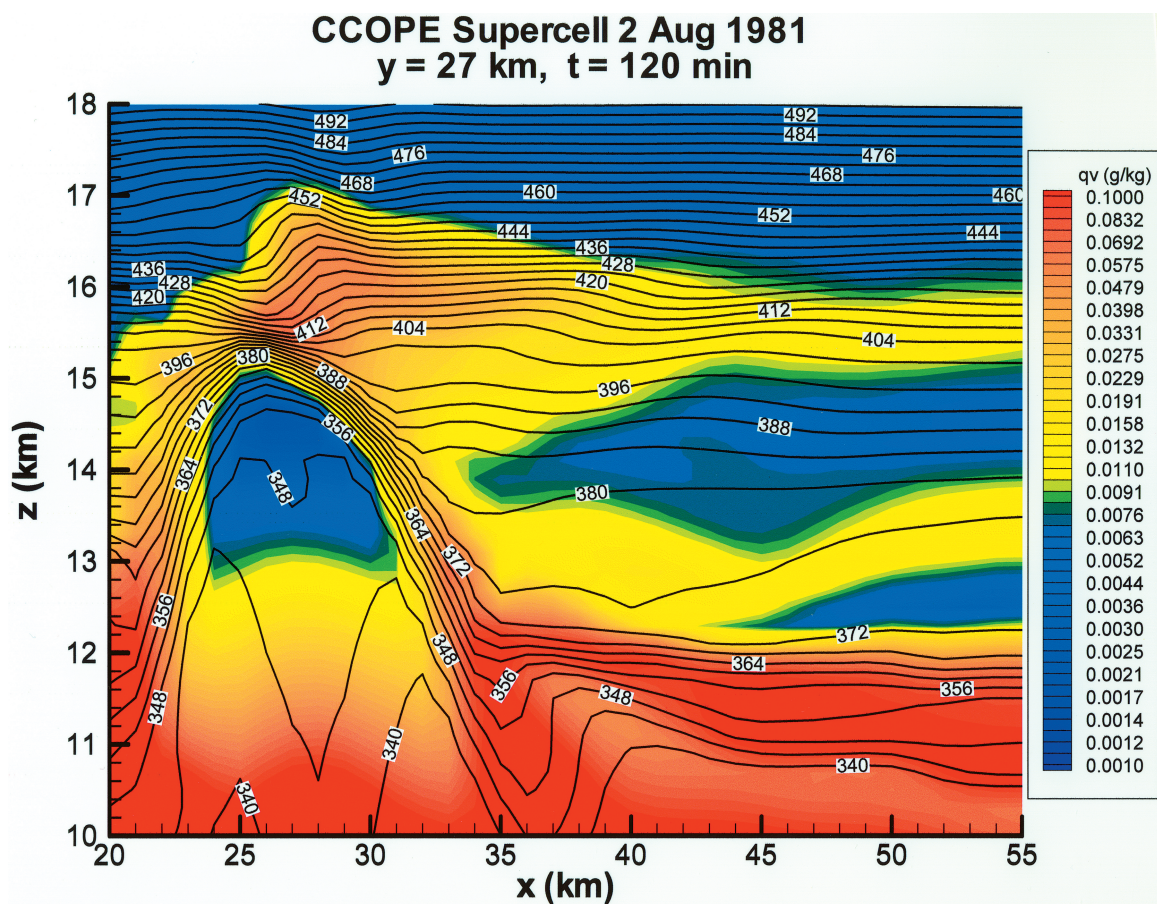


Figure 6. Central east-west cross-section of the simulated storm at $t = 120$ min showing the overlapped q_v and θ fields.

[40] Obviously, the moisture in the dome shell comes from the troposphere, as there is very little water vapor in the stratosphere to serve as a source. In fact, the moisture content of the dome shell would have been higher if it had not mixed with the warmer and drier stratospheric air.

[41] The values of q_v in the plumes core fluctuates between $0.3 \sim 0.6 \text{ g kg}^{-1}$ (about $50 \sim 100$ ppm). Even though the plume is low in water vapor, it is still more humid than the surrounding stratosphere whose water vapor concentration is typically $2 \sim 3$ ppm. The plumes undoubtedly serve to moisturize the stratosphere.

4.5. Enhancement of Turbulent Mixing by Wave Breaking

[42] What is the mechanism that is responsible for this diabatic exchange? It cannot be due to pure gravity wave motions as they are an adiabatic process. It is not radiative heating either as it is not included in the model. The main mechanism is most likely the turbulent mixing of the dome air with the warmer and drier stratospheric air, which will unquestionably result in the higher potential temperatures in the plume. Overshooting dome results in some mixing between cloudy air and stratospheric air. Interfacial instabilities, resulting from the strong shear near the dome interface, lead to some exchange between the dome and its environment. These instabilities are similar to those

studied by *Grabowski and Clark* [1991, 1993a, 1993b]. This process involves moist thermodynamics, and latent heating has some effect. The major modification of this process comes from breaking gravity waves, which can pull the air from either the dome or the anvil. Turbulent mixing readily occurs even without the gravity wave breaking, but will be dramatically enhanced by the wave breaking. This breaking-enhanced turbulent mixing is the mechanism responsible for the plume formation.

5. Observational Evidence of the Anvil Top Plume Phenomenon

[43] The plume phenomenon as described above has been reported previously in aircraft and satellite observations, although its nature and formation mechanism were unclear at the time. *Roach* [1967] and *Fujita* [1982] pointed out observations of cirrus clouds atop the anvils of some severe thunderstorms, and mentioned that collapsing overshooting tops produced them, although they did not identify the source of water vapor. More recently, *Setvak and Doswell* [1991] and *Levizzani and Setvak* [1996] reported the observation of plume features on top of some convective storms in Advanced Very High Resolution Radiometer (AVHRR) satellite imagery of the US National Oceanographic and Atmospheric Administration (NOAA) polar orbiters. Examples of the anvil-top plumes are shown in Figure 9. These

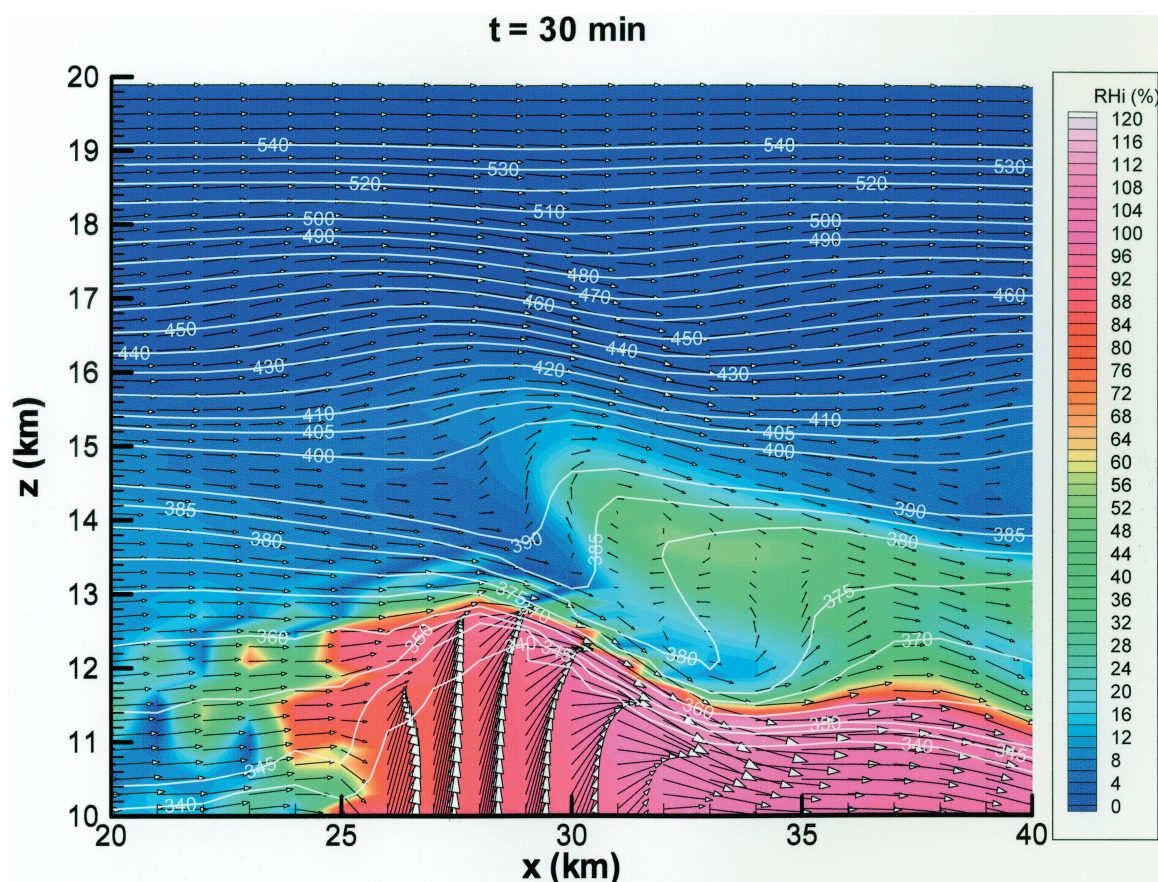


Figure 7. Central east-west cross-section of the simulated storm at $t = 30$ min, showing the overlapped RH, wind vector (projected on the x - z plane) and θ fields. The wave breaking is obvious in the region where $x \sim 33$ km and $z \sim 12.5$ km.

studies were based on the AVHRR channels 2 ($0.625\text{--}1.1\ \mu\text{m}$), 3 ($3.55\text{--}3.93\ \mu\text{m}$), and 4 ($10.3\text{--}11.3\ \mu\text{m}$) but some visible characteristics in channel 1 (visible) are also included. Major characteristics that are common to these plumes are as follows [Levizzani and Setvak, 1996]: (1) A small bright spot in channel 2 a few pixels across, i.e., a few kilometers, in the form of an oval cloud, is detected as the plume's source. The shadow cast by this rounded cloud appears much longer than that of the plume, suggesting a higher altitude. The source spot is normally shifted downwind from the coldest area, and collocated with the storm's embedded warm area. (2) These cloud plumes spread downwind, usually along the central axis of the storm anvil, resembling smoke plumes from a chimney. The estimated height in one case is about 15 km. (3) They are vertically separated from the underlying anvils, as deduced from the shadows they cast on the anvils. (4) Plumes are partially transparent in channels 1 and 2, and one can often see through them and discern some features on the underlying anvil. This indicates that the plumes are usually very thin and tenuous. (5) The structure of the plume is more or less preserved in channel 4, indicating a temperature difference between the particles of the plume and the surroundings.

[44] All these features are essentially reproduced by the present model results. This lends support to the mechanism proposed in this paper. Levizzani and Setvak [1996] stated that the mechanism of plume formation is unclear. They

indicated that the plumes do not seem to be associated with wave motions, as they do not exhibit wave cloud characteristics. The present model results suggest that the plumes form from the water vapor ejected by the storm cloud via the gravity wave breaking-enhanced turbulent mixing, as described in the previous section.

6. Cross-Tropopause Transport of Water Vapor by Plumes

[45] The anvil top plume phenomenon implies that water vapor is transported from the moister troposphere to the drier stratosphere, hence playing a role of moisturizing the stratosphere. Roach [1967] suggested that the rate of exchange between the troposphere and stratosphere due to the overshooting is probably small compared to the total flux of air through the storm system. Whereas this statement is true, it is increasing recognized that even a small amount of water vapor in the stratosphere may have important implications to the global climate and atmospheric chemistry systems. Thus it is necessary to carefully estimate the plume transport of water vapor.

[46] It is not straightforward to define where the tropopause is in a strong convective region, and we choose the 375K equivalent potential temperature (θ_e) surface as the tropopause here because it appears to coincide approximately with the cloud top based on inspection of the

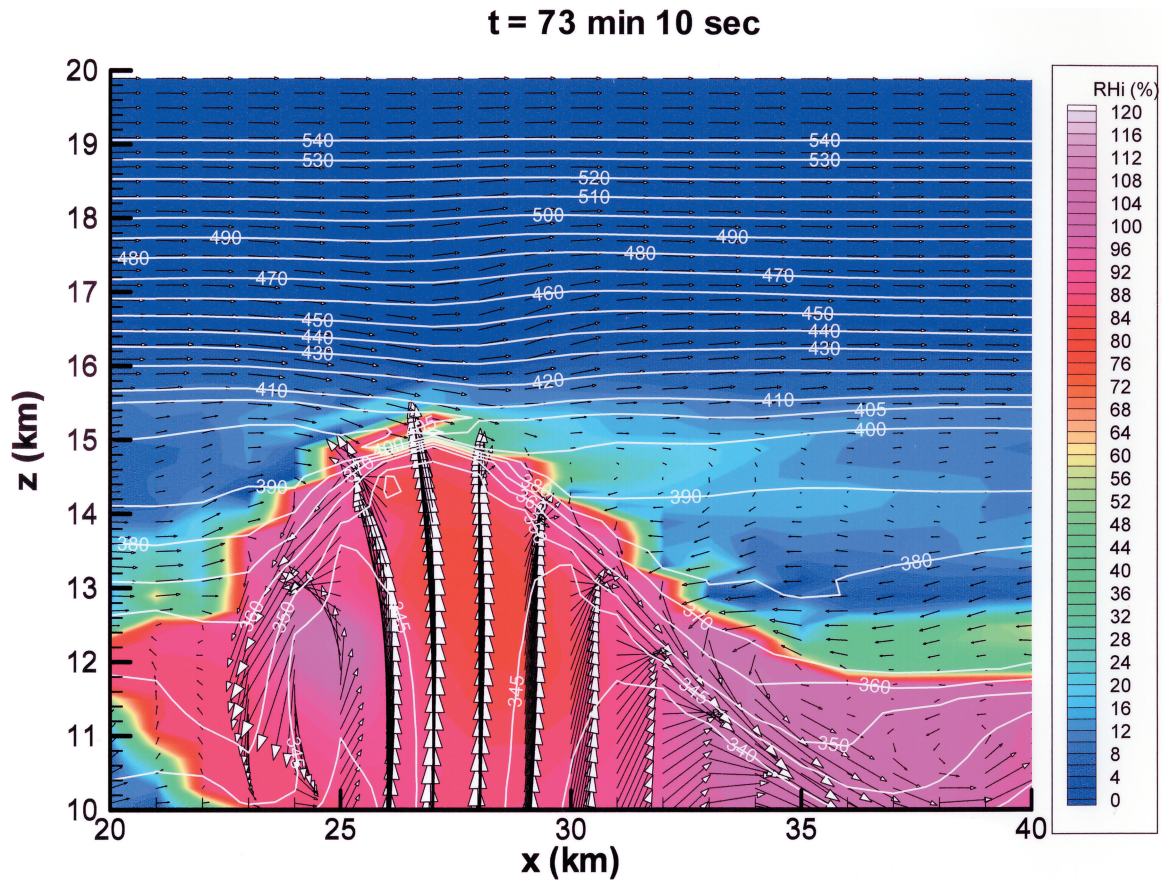


Figure 8. Central east-west cross-section of the simulated storm at $t = 73$ min 10 sec, showing the overlapped RH, wind vector (projected on the x - z plane) and θ fields. The wave breaking is obvious in the region where $x \sim 28$ km and $z \sim 15$ km.

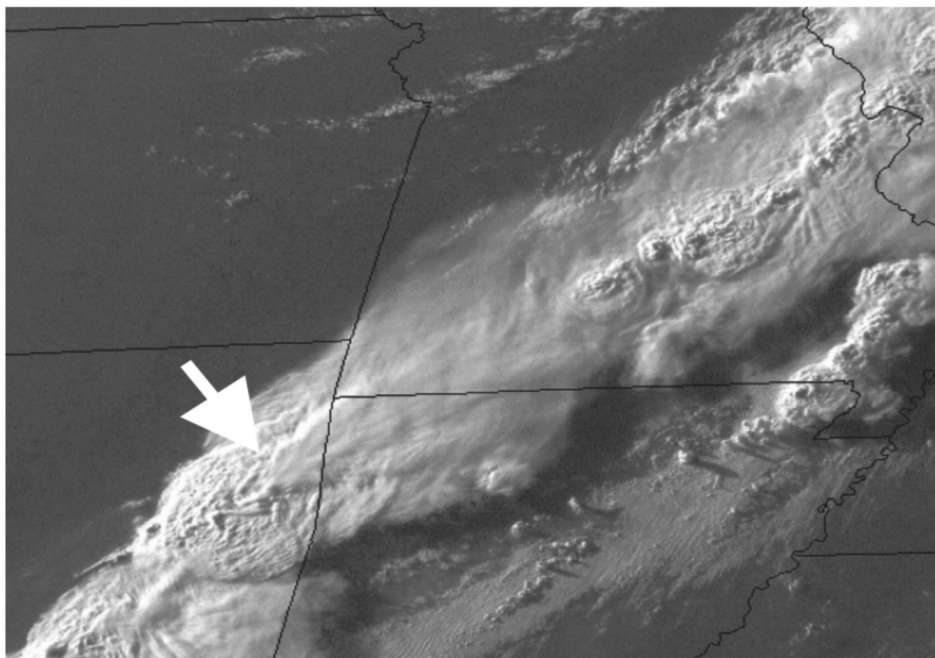


Figure 9. A composite of channels 1, 2 and 4 of 1 June 1999 0015 UTC NOAA GOES-8 satellite image depicting an extensive line of thunderstorms in the Plains. A plume is clearly visible on top of the anvil of the storm cell near the northeastern corner of Oklahoma. (NOAA).

animation of the RH_i profile. Naturally, this should be regarded as an approximation only, as in reality this θ_e surface can deviate from the cloud top from time to time. Because of this and other uncertainties, the following estimates should be taken in the sense of order-of-magnitude only.

[47] The transport of water vapor due to the plume phenomenon described above is calculated by summing the values of $\rho q_v \mathbf{V} \cdot \mathbf{A}$ at all grid points on the 375K θ_e -surface where the plume appears. This quantity represents the vapor flux that crosses this θ_e -surface and enters the stratosphere. Here ρ is the air density, \mathbf{V} the wind vector on the grid, and \mathbf{A} the surface of the grid boxes involved. The resulting water vapor flux versus time is plotted in Figure 10, which shows that the upward transport of water vapor occurs in pulses. The average vapor flux during this period is about 3 tons/sec. It is unclear at present whether this value is typical for all severe storms or specific to this storm. There is clearly an urgent need to perform more observational and theoretical studies to make better estimates of this quantity.

[48] Since the current simulation ends at $t = 150$ min for the storm, it is not long enough to study the fate of the water vapor. The water vapor may continue to be transported in the stratosphere and become involved in chemical reactions and destroyed, or they may be transported back to the troposphere by turbulent diffusion or other removal processes. One path that the plume water vapor returns to the troposphere is that they form ice crystals and fall out from the stratosphere if they are large enough. While the properties of the water vapor plumes in the simulated storm match those of the observed plumes in almost every aspect, there is one discrepancy: only very small amount of ice particles are produced in the plume. The maximum cloud ice and snow mixing ratios in the simulated plumes are typically between 0.002 to 0.005 g kg^{-1} . It is felt that there should be more ice crystals than the simulated values since the plumes are sometimes detected in visible wavelengths, albeit very tenuous. The lack of adequate ice particles in the modeled plumes is most likely due to the inadequacy of the parameterizations in the formation of ice particles. Present ice parameterizations have been experimentally tested only for temperatures down to -40°C whereas the temperatures in the plumes are about -65°C or colder.

[49] Recent model studies of subvisual cirrus clouds near the tropical tropopause indicate that ice crystals in such high altitudes are unlikely to exceed a few microns in size [Jensen and Toon, 1994; Jensen et al., 1996a, 1996b]. Such small ice crystals will fall very slowly, being typically a few tenths of 1 cm s^{-1} . Even at 1 cm s^{-1} , it will take these ice crystals 10^5 sec (longer than one day) to fall 1 km. Thus the most likely fate of these ice crystals is to sublimate to vapor. If the midlatitude plume ice crystals have size similar to those in the tropical cirrus, then they too would sublimate before they fall back to the troposphere. Sublimation is made even more likely because the plume temperatures are typically warmer than the tropical tropopause ($\sim -85^\circ\text{C}$).

[50] We can make a very crude estimate of the global water vapor transport from the troposphere to the stratosphere if we assume for the moment that a typical thunderstorm cell would transport 3 tons/s of water vapor. If we further assume that there are ~ 2000 active thunderstorm

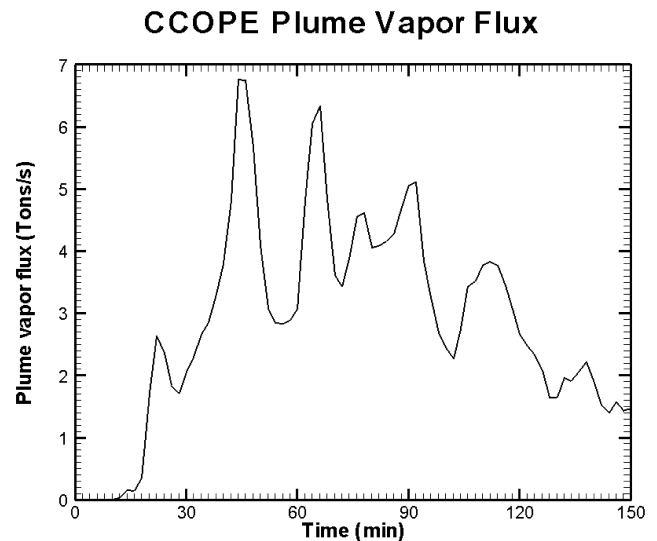


Figure 10. Time series of water vapor flux through the $\theta_e = 375$ K surface for the simulated storm.

cells globally (including both midlatitude and tropical cases in both hemispheres) at any given time [Mason, 1971; Volland, 1984] and that each thunderstorm behaves more-or-less the same as the one simulated here, then the global UT to LS transport of water vapor would be about 6000 tons/s or 5.18×10^8 tons/day, roughly half a billion tons per day. At present it is difficult to assess the uncertainty of this estimate, as we do not know how thunderstorms in different geographical locations differ in the plume transport. Not all thunderstorms are severe and tropical thunderstorms may behave differently from the midlatitude storms. Even if it is in the proper order of magnitude, how important this quantity is to the global lower stratospheric water vapor budget depends on many other complicated factors such as where and how this water vapor is distributed, the details of local circulations, and how it interacts with other chemical species. There is clearly a need to perform more studies to answer this question.

[51] It is also noted that the water vapor transport in this case is into the lowermost stratosphere. At present we are unclear about the fate of this water vapor. Questions such as whether or not it will precipitate out in regions further downstream of the storm, or be destroyed locally by chemical reactions, or be transported upward into higher stratosphere must await further studies.

7. Conclusions and Outlook

7.1. Overview

[52] In this paper, a hypothesis is advanced to explain the plume features above the anvils of certain severe thunderstorms, as observed by meteorological satellites. The results from a numerical simulation of a deep convective system, a supercell storm that occurred in the US High Plains in August 1981, were analyzed to search for clues to the plume formation mechanisms. Our analysis shows that the primary water vapor source for these plumes is most likely the shell of the storm's overshooting dome. The vigorous vertical motions in the updraft core set up vigorous gravity waves.

When instability becomes sufficiently large, wave breaking occurs and masses are transferred through isentropic surfaces. The tropospheric water vapor thus become injected into the stratosphere and is carried downwind by the upper-level winds, forming a shape like a chimney plume. As shown in the preceding sections, the characteristics of the modeled moisture plumes fit well with most major characteristics of the observed plumes. However, the model did not predict sufficiently high ice crystal concentrations that can be visualized, whereas the satellite observations did show plumes in visible channels. This discrepancy is most likely due to the deficiencies in the parameterizations of ice crystal formation in the model. Unfortunately, our current knowledge of ice formation in the temperature range prevalent in the cloud top region is inadequate, and there is a need to perform observations and/or laboratory experiments to provide such information.

[53] The hypothesized plume mechanism also explains qualitatively the seasonal variations and the hemispheric asymmetry of lower-stratospheric (LS) water vapor concentrations in midlatitudes as deduced from satellite data. However it is still uncertain whether this mechanism also explains them quantitatively. A larger scale model, perhaps a global circulation model, equipped with good parameterizations of cross-tropopause water vapor transport, will be necessary to make better assessments of water vapor transport and explain the observed LS water vapor field quantitatively.

[54] If the hypothesis is proved correct, then it implies that there is a water vapor source that should go into the global water vapor transport scheme. It is uncertain at present how significant this source is. If it turns out to be significant, then it may be necessary to make a better assessment of its impact on climate, in view of the capability water vapor to absorb infrared radiation.

[55] Most works concerning stratosphere-troposphere exchange assume that the exchange is achieved mostly via the way of isentropic mixing. This work indicates that the convective process may not be negligible as previously thought. Since the chemical composition of the air is latitude dependent, the isentropic mixing and convective transport mechanisms will likely bring different chemical composition into the lower stratosphere.

[56] One of the implications of this mechanism is the transport of other trace chemicals into the stratosphere. Due to the low temperature of the tropopause, water vapor is subject to efficient removal by condensation/freezing that hinders its upward transport. Therefore, if water vapor can be transported from the troposphere to the stratosphere by the plume mechanism, then other trace chemicals can do so as well. This is especially true for chemicals with low condensation/freezing point temperatures and small water solubility under the tropopausal conditions. Several trace gases of importance to atmospheric chemistry, for example, ozone and chlorofluorocarbons (CFC's), as well as some natural and anthropogenic aerosol particles possess such chemical properties. We have performed a few test runs of inert tracer transport by deep convective systems using the same model storm as described in section 4 and assuming that the tracer is initially uniformly distributed in the lowest km. Preliminary analysis of the results (not shown) indicates that the tracer can be transported even

higher up into the stratosphere than can water vapor, confirming the above statement. This means that the anvil-top plume mechanism can be important to stratospheric/tropospheric exchange of key atmospheric chemicals and deserves further investigation.

7.2. Future Simulation Studies

[57] The estimate of upward water vapor flux given in the section 6 should be regarded as preliminary, as it may vary from storm to storm depending on their specific dynamical and physical conditions. We are making plans to perform sensitivity studies of plume vapor transport under various sounding and wind shear conditions as well as grid resolutions.

[58] Furthermore, it is known that grid resolution may have significant impact on the model results for convection. This is especially true near sharp boundaries, such as cloud edges and the tropopause. The quantitative aspect of adiabatic versus diabatic transport discussed in this paper may be influenced by model parameters such as the grid resolution, the turbulence closure and the advection schemes. Future sensitivity studies are being planned to investigate the impact of model resolution by using finer grid spacings, especially in the vertical direction, to see whether or not the estimates made above are stable within a reasonable range. Also to be studied are the impact of resolved versus parameterized transport processes and the role of numerical diffusion by using different subgrid scale parameterizations and the advection schemes.

[59] **Acknowledgments.** I am grateful to Susan Solomon for pointing out relevant references and for her encouraging and helpful comments, to Liwen Pan for sharing the SAGE II data, to Yuh-Lang Lin, Bill Hall, Todd Lane, and Bob Sharman for discussion of gravity waves, to Hsinmu Lin and Yulien Chu for help processing the model data, and to Robert Schlesinger for helpful comments. Three anonymous reviewers have given the author many helpful comments that led to improvement of the paper. This study was first inspired by a discussion with Vincenzo Levizzani and Martin Setvak. This work is partially supported by NSF grants ATM-9907761 and ATM-9633424 and NASA grant NAG5-7605.

References

- Alexander, M. J., J. R. Holton, and D. R. Durran, The gravity wave response above deep convection in a squall line simulation, *J. Atmos. Sci.*, 52, 2212–2226, 1995.
- Anderson, J. R., K. K. Droegemeier, and R. B. Wilhelmson, Simulation of the thunderstorm subcloud environment, paper presented at Conference on Severe Local Storms, Am. Meteorol. Soc., Indianapolis, Indiana, 1985.
- Arakawa, A., and V. R. Lamb, A potential enstrophy conserving scheme for the shallow water equations, *Mon. Weather Rev.*, 109, 18–36, 1981.
- Asselin, R., Frequency filter for time integrations, *Mon. Weather Rev.*, 100, 487–490, 1972.
- Chen, P., Isentropic cross-tropopause mass exchange in the extratropics, *J. Geophys. Res.*, 100, 16,661–16,673, 1995.
- Clark, T. L., T. Hauf, and J. P. Kuettner, Convectively forced internal gravity waves: Results from two-dimensional numerical experiments, *Q. J. R. Meteorol. Soc.*, 112, 899–925, 1986.
- Cotton, W. R., M. A. Stephens, T. Nehrkorn, and G. J. Tripoli, The Colorado State University three-dimensional cloud model – 1982, part II, An ice phase parameterization, *J. Rech. Atmos.*, 16, 295–320, 1982.
- Cotton, W. R., G. J. Tripoli, R. M. Rauber, and E. A. Mulvihill, Numerical simulation of the effects of varying ice crystal nucleation rates and aggregation processes on orographic snowfall, *J. Clim. Appl. Meteorol.*, 25, 1658–1680, 1986.
- Danielsen, E. F., In situ evidence of rapid, vertical irreversible transport of lower tropospheric air into the lower tropical stratosphere by convective cloud turrets and by large-scale upwelling in tropical cyclones, *J. Geophys. Res.*, 98, 8665–8681, 1993.

- Dunkerton, T. J., Evidence of meridional motion in the summer lower stratosphere adjacent to monsoon regions, *J. Geophys. Res.*, *100*, 16,675–16,688, 1995.
- Federer, B., and A. Waldvogel, Hail and raindrop size distributions from a Swiss multicell storm, *J. Appl. Meteorol.*, *14*, 91–97, 1975.
- Foot, J. S., Aircraft measurements of the humidity in the lower stratosphere from 1977 to 1980 between 45N and 65N, *Q. J. R. Meteorol. Soc.*, *110*, 303–319, 1984.
- Fovell, R., D. Durran, and J. R. Holton, Numerical simulation of convectively generated stratospheric gravity waves, *J. Atmos. Sci.*, *49*, 1427–1442, 1992.
- Fujita, T. T., Principle of stereographic height computations and their application to stratospheric cirrus over severe thunderstorms, *J. Meteorol. Soc. Japan*, *60*, 355–368, 1982.
- Goody, R. M., and Y. L. Yung, *Atmospheric Radiation: Theoretical Basis*, Oxford Univ. Press, New York, 1989.
- Grabowski, W. W., and T. L. Clark, Cloud-environment interface instability: Rising thermal calculations in two spatial dimensions, *J. Atmos. Sci.*, *48*, 527–546, 1991.
- Grabowski, W. W., and T. L. Clark, Cloud-environment interface instability, part II, Extension to three spatial dimensions, *J. Atmos. Sci.*, *50*, 555–573, 1993a.
- Grabowski, W. W., and T. L. Clark, Cloud-environment interface instability, part III, Direct influence of environmental shear, *J. Atmos. Sci.*, *50*, 3821–3828, 1993b.
- Gunn, K. L. S., and J. S. Marshall, The distribution with size of snow aggregates, *J. Meteorol.*, *15*, 452–461, 1958.
- Hints, E. J., E. M. Weinstock, A. E. Dessler, J. G. Anderson, M. Lowenstein, and J. R. Podolske, SPADE H₂O measurements and the seasonal cycle of stratospheric water vapor, *Geophys. Res. Lett.*, *21*, 2559–2562, 1994.
- Holton, J. R., P. H. Haynes, M. E. McIntyre, A. R. Douglass, R. B. Rood, and L. Pfister, Stratospheric-tropospheric exchange, *Rev. Geophys.*, *33*, 403–439, 1995.
- Jensen, J. E., and O. B. Toon, Ice nucleation in the upper troposphere: Sensitivity to aerosol number density, temperature, and cooling rate, *Geophys. Res. Lett.*, *21*, 2019–2022, 1994.
- Jensen, J. E., O. B. Toon, L. Pfister, and H. B. Selkirk, Dehydration of the upper troposphere and lower stratosphere by subvisual cirrus clouds near the tropical tropopause, *Geophys. Res. Lett.*, *23*, 825–828, 1996a.
- Jensen, J. E., O. B. Toon, H. B. Selkirk, J. D. Spinhirne, and M. R. Schroebel, On the formation and persistence of subvisual cirrus clouds near the tropical tropopause, *J. Geophys. Res.*, *101*, 21,361–21,375, 1996b.
- Johnson, D. E., P. K. Wang, and J. M. Straka, Numerical simulation of the 2 August 1981 CCOPE supercell storm with and without ice microphysics, *J. Appl. Meteorol.*, *32*, 745–759, 1993.
- Johnson, D. E., P. K. Wang, and J. M. Straka, A study of microphysical processes in the 2 August 1981 CCOPE supercell storm, *Atmos. Res.*, *33*, 93–123, 1994.
- Kelly, K. K., A. F. Tuck, L. E. Heidt, M. Loewenstein, J. R. Poldoske, S. E. Strahan, and J. F. Vedder, A comparison of ER-2 measurements of stratospheric water vapor between the 1987 Antarctic and 1989 Arctic Airborne Missions, *Geophys. Res. Lett.*, *17*, 465–468, 1990.
- Klemp, J. B., and R. B. Wilhelmson, The simulation of three-dimensional convective storm dynamics, *J. Atmos. Sci.*, *35*, 1070–1096, 1978a.
- Klemp, J. B., and R. B. Wilhelmson, Simulations of right- and left-moving storms produced through storm-splitting, *J. Atmos. Sci.*, *35*, 1087–1110, 1978b.
- Knight, C. A., The Cooperative Convective Precipitation Experiment (CCOPE), 18 May–7 August 1981, *Bull. Am. Meteorol. Soc.*, *63*, 386–398, 1982.
- Levizzani, V., and M. Setvak, Multispectral, high resolution satellite observations of plumes on top of convective storms, *J. Atmos. Sci.*, *53*, 361–369, 1996.
- Lin, Y. L., R. D. Farley, and H. D. Orville, Bulk parameterization of the snow field in a cloud model, *J. Clim. Appl. Meteorol.*, *22*, 1065–1092, 1983.
- Liou, K. N., *Radiation and Cloud Processes in the Atmosphere: Theory, Observation, and Modeling*, 487 pp., Oxford Univ. Press, New York, 1992.
- Marshall, J. S., and M. Palmer, The distribution of raindrops with size, *J. Meteorol.*, *5*, 165–166, 1948.
- Mason, B. J., *The Physics of Clouds*, Clarendon, Oxford, England, 1971.
- Miller, L. J., D. Tuttle, and C. A. Knight, Airflow and hail growth in a severe northern High Plains supercell, *J. Atmos. Sci.*, *45*, 736–762, 1988.
- Oltmans, S. J., H. Volmer, D. J. Hofman, K. H. Rosenlof, and D. Kley, The increase in stratospheric water vapor from balloonborne, frostpoint hygrometer measurements at Washington, D. C., and Boulder, Colorado, *Geophys. Res. Lett.*, *27*, 3453–3456, 2000.
- Pan, L., S. Solomon, W. Randel, J.-F. Lamarque, P. Hess, J. Gille, E. Chiou, and M. P. McCormick, Hemispheric symmetries and seasonal variations of the lowermost stratospheric water vapor and ozone derived from SAGE II data, *J. Geophys. Res.*, *102*, 28,177–28,184, 1997.
- Pandya, R. E., and M. J. Alexander, Linear stratospheric gravity waves above convection thermal forcing, *J. Atmos. Sci.*, *56*, 2434–2446, 1999.
- Plumb, R. A., and J. Eluszkiewicz, The Brewer-Dobson circulation: Dynamics of the tropical upwelling, *J. Atmos. Sci.*, *56*, 868–890, 1999.
- Roach, W. T., On the nature of the summit areas of severe storms in Oklahoma, *Q. J. R. Meteorol. Soc.*, *93*, 318–336, 1967.
- Rosenlof, K. H., A. F. Tuck, K. K. Kelly, J. M. Russell III, and M. P. McCormick, Hemispheric asymmetry in water vapor and inference about transport in the lower stratosphere, *J. Geophys. Res.*, *102*, 13,213–13,234, 1997.
- Setvak, M., and C. A. Doswell III, The AVHRR channel 3 cloud top reflectivity of convective storms, *Mon. Weather Rev.*, *119*, 841–847, 1991.
- Solomon, S., Stratospheric ozone depletion: A review of concept and history, *Rev. Geophys.*, *37*, 275–316, 1999.
- Straka, J. M., Hail growth in a highly glaciated central high plains multicellular hailstorm, Ph.D. thesis, 413 pp., Univ. of Wisc.-Madison, 1989.
- Tremback, C., J. Powell, W. R. Cotton, and R. A. Pielke, The forward-in-time upstream advection scheme: Extension to higher order, *Mon. Weather Rev.*, *115*, 540–555, 1987.
- Volland, H., *Atmospheric Electrodynamics*, Springer-Verlag, New York, 1984.
- Wade, C. G., A preliminary study of an intense thunderstorm which move across the CCOPE research network in southeastern Montana, paper presented at Ninth Conference on Weather Forecasting and Analysis, Am. Meteorol. Soc., Seattle, Wash., 1982.
- Weisman, M. L., and J. B. Klemp, The dependence of numerically simulated convective storms on the vertical wind shear and buoyancy, *Mon. Weather Rev.*, *110*, 504–520, 1982.
- Weisman, M. L., J. B. Klemp, and L. J. Miller, Modeling and Doppler analysis of the CCOPE August 2 supercell storm, paper presented at 13th Conference on Severe Local Storms, Am. Meteorol. Soc., Tulsa, Okla., 1983.

P. K. Wang, Department of Atmospheric and Oceanic Sciences, University of Wisconsin-Madison, Madison, WI 53706, USA. (pao@windy.meteor.wisc.edu)